WIDESEE: Towards Wide-Area Contactless Wireless Sensing

Lili Chen[†,‡], Jie Xiong[§], Xiaojiang Chen[†,‡], Sunghoon Ivan Lee[§], Kai Chen[†,‡]
Dianhe Han[†,‡], Dingyi Fang[†,‡], Zhanyong Tang[†,‡], Zheng Wang[$]

[†]Northwest University, [‡]International Joint Research Centre for Battery-free IoT
[§]University of Massachusetts Amherst, [$]University of Leeds

ABSTRACT

Contactless wireless sensing without attaching a device to the target has achieved promising progress in recent years. However, one severe limitation is the small sensing range. This paper presents WIDESEE to realize wide-area sensing with only one transceiver pair. WIDESEE utilizes the LoRa signal to achieve a larger range of sensing and further incorporates drone's mobility to broaden the sensing area. WIDESEE presents solutions across software and hardware to overcome two aspects of challenges for wide-range contactless sensing: (i) the interference brought by the device mobility and LoRa's high sensitivity; and (ii) the ambiguous target information such as location when employing just a single pair of transceivers. We have developed a working prototype of WIDESEE for human target detection and localization that are especially useful in emergency scenarios such as rescue search, and evaluated WIDESEE with both controlled experiments and the field study in a high-rise building. Extensive experiments demonstrate the great potential of WIDESEE for wide-area contactless sensing with a single LoRa transceiver pair hosted on a drone.

CCS CONCEPTS

• **Human-centered computing** → **Ubiquitous and mobile computing**; • **Hardware** → *Communication hardware, interfaces and storage*.

KEYWORDS

Wide-area; Wireless sensing; LoRa; Mobility

ACM Reference Format:
Lili Chen[†,‡], Jie Xiong[§], Xiaojiang Chen[†,‡], Sunghoon Ivan Lee[§], Kai Chen[†,‡] and Dianhe Han[†,‡], Dingyi Fang[†,‡], Zhanyong Tang[†,‡], Zheng Wang[$]. 2019. WIDESEE: Towards Wide-Area Contactless Wireless Sensing. In *The 17th ACM Conference on Embedded Networked Sensor Systems (SenSys '19), November 10–13, 2019, New York, NY, USA.* ACM, New York, NY, USA, 13 pages. https://doi.org/10.1145/3356250.3361931

Corresponding author: Xiaojiang Chen (xjchen@nwu.edu.cn)

SenSys '19, November 10–13, 2019, New York, NY, USA

ACM ISBN 978-1-4503-6950-3/19/11…$15.00
https://doi.org/10.1145/3356250.3361931

1 INTRODUCTION

Besides traditional data communication functions, in recent years, wireless signals have been employed for sensing and have enabled diverse new applications including indoor navigation [22, 51, 54], health monitoring [9, 39], and human-computer interactions [14]. Wireless sensing relies on analyzing the characteristics of the signal reflected from the target to understand the contextual information of one's interest (e.g., localization). A wide range of wireless signals have been exploited for contactless sensing (i.e., without attaching any device to the target objects), including ultrasound and various types of radio frequency (RF) signals (e.g., WiFi and RFID). The RF signals attract particular attention in real-world sensing applications since they do not require to secure a Line-of-Sight (LoS) between the device and targets as opposed to conventional camera-based systems [37], and have stronger penetration capability compared to acoustic signals [43, 50].

Although promising, one evident issue with existing RF-based sensing is its limited sensing range, which hinders its applications in wide-area sensing such as disaster rescue. This is mainly because the signals reflected from the target, which contain information related to the context of the target, are much weaker than the direct-path signals between the transmitter and receiver. The fact that wireless sensing captures information from the reflected signals makes the sensing range much smaller compared to when the signals are used for communication purposes. For example, the current WiFi-based systems are only capable of performing sensing in a room-level range (i.e. approximately 3-6 m) [26, 51], whereas RFID or mmWave-based systems show an even smaller sensing range of 1-3 m [27, 47, 55].

Recently, efforts have been made to extend the contact sensing range of RF signals [11, 24, 56, 57]. Ashutosh *et al.* introduced an approach to employ multi-hop nodes to track the sensor attached targets that are located deep inside a building structure [11]. In another example, Ma *et al.* leveraged drones to relay sensing information, which extends the sensing range from 5 m to 50 m [57]. Employing multiple devices or multi-hop transmission schemes can increase the sensing coverage range. However, these approaches require a complicated process of sensing infrastructure deployment and could be vulnerable to changes or failure of even a single device, which make them unsuitable for emergency rescue applications.

In this paper, we present WIDESEE– a contactless wireless sensing system based on the emerging LoRa technology *with only a single transceiver pair*. WIDESEE is designed to push the boundary of wide-area sensing. Our key insight is that the low-power, long-range wireless communication capability of LoRa offers a long

propagation distance (i.e., several kilometers) and a strong penetration capability through obstacles, which in turn can be employed to significantly increase the sensing range compared to other wireless technologies. In this work, as a proof-of-concept, we explore the opportunities and limitations of the LoRa technology for non-contact human detection and localization in wide-area scenarios. To further increase the sensing area coverage, we leverage the mobility of a drone to carry the transceiver and move around the target area to perform wireless sensing. As we demonstrate later in this paper, we successfully realize building-scale, through-wall sensing to detect and localize human targets. We believe the proposed study is particularly useful for human target sensing (detection and localization) for applications in urban search and rescue missions.

Translating our high-level idea into a functional system, however, is nontrivial due to a number of challenges. First, the larger sensing range of LoRa also means the interference range is also larger due to the higher signal receiving sensitivity. Second, a transceiver pair equipped with a single antenna does not provide us sufficient information regarding the target location since the number of unknown variables is greater than that of the constrained equations for localization. Third, although employing a drone can increase the sensing coverage, the vibration introduced by the drone during its operation (i.e., flying) affects the resultant signals and accordingly the target sensing performance.

To address the aforementioned challenges in wide-range sensing, we introduce solutions across the software and hardware stacks. To tackle the interference brought by LoRa's high sensitivity, we redesign the antenna system and the sensing algorithm. Specifically, we employ a compact, reconfigurable directional antenna at the receiver to narrow down the target sensing region. Our system can quickly (i.e., within 10 ms) switch the radiation pattern with a narrow beamwidth of 48°. Such a design allows WIDESEE to stay focus on the area of interests and reduce the impact of interference. To further eliminate the multipath effect within the sensing area, we take a unique approach to first extract the direction-related information from available time-series of amplitudes and then use the information to isolate the target path from the interfering multipath. As a departure from the commonly used angle-of-arrival (AoA) or time-of-flight (ToF)-based methods, our design avoids the pitfall of relying on accurate channel phase information and large bandwidth, which are unfortunately not available on LoRa.

To reduce the ambiguities in localization, we build analytic models that can predict and determine target locations. This is based on our key observations that the speed of the moving target (e.g., humans) is relatively constant and the resulting trajectory is smooth within a short period of time (e.g., $< 1\ s$). We model the signal characteristics of the (vibration) noise and human target movements in frequency domain and filter out the vibration artifacts on the received signals to improve the sensing accuracy.

We integrate the proposed techniques to implement a working prototype and deploy it to detect and localize human targets in three different real-world environments: an open square, an underground parking garage, and a high-rise building structure with a size of $20 \times 42 \times 85\ m^3$. Our experimental results show that WIDESEE can effectively detect and localize human targets using just one transceiver pair. For 90% of the test cases, the localization error of WIDESEE is within 4.6 m. Such accuracy would allow one to identify at which room the human target locates in many typical building structures. This is a promising result considering we use only a single transceiver pair, and the target moves most of the time in a large environment. We hope this study can encourage further research in exploiting wide-area wireless sensing in detecting and tracking human targets to enable applications like disaster rescue search and security surveillance [48]. The main contributions of this paper can be summarized as followings:

Figure 1: Motivation example of WIDESEE: a building-scale human target sensing scenario.

- We present a contactless system for sensing human targets in a wide area using just one transceiver pair, by combining the agility of drone with the long-range propagation characteristic of LoRa.
- We introduce new algorithms and design methodologies across the software and hardware stacks to effectively tackle a series of interference issues when applying LoRa and a flying drone for wide-range sensing, and to address the sensing ambiguity issue when only one single transceiver pair is employed. The proposed techniques are generally applicable, and can be applied to other wireless sensing tasks.
- We demonstrate, for the first time, building-scale, through-wall contactless wireless sensing can be achieved with just one LoRa transceiver pair together with a drone.

2 BACKGROUND AND OVERVIEW

2.1 LoRa Technology

LoRa offers a long communication range for up to several kilometers [45] with the ability to decode signals as weak as $-148\ dBm$. While the ability of decoding weak signals is beneficial for long range communications, it makes LoRa more likely to suffer interference from uninterested area in sensing. Even using a directional antenna at the receiver, there still exist strong multipath effects [30] within the detectable area that greatly affect the sensing accuracy. Much effort has been made to similar problems associated with multipath effects in other RF signals (e.g., WiFi [49] or RFID [58]) or acoustic signals [43], which are based on AoA or ToF information of the received signals. However, such information requires accurate channel phase readings and clock synchronization between the transmitter and receiver, both of which are unavailable on LoRa.

In this work, instead of making efforts on obtaining AoA or ToF to tackle the multipath effects, we consider a approach to leverage the received (albeit susceptible) signal strength (i.e., amplitude) for effectively addressing the inherent issue of multipath effects. This is described in Section 3.3.

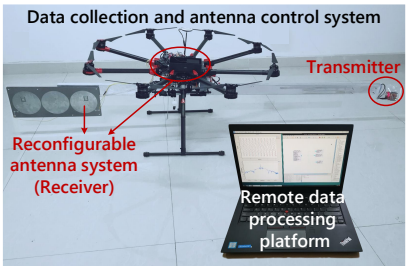

Figure 2: Overview of WIDESEE. We use a drone to carry the LoRa transceiver pair and its control system. The data are sent back to the remote data processing platform to perform real-time target detection and localization.

2.2 Motivation and Problem Scope

As depicted in the conceptual illustration in Figure 1, WIDESEE could be used to target emergency scenarios, such as disaster rescue and terrorist search in (high-rise) building structures. In these scenarios, identification of the presence of human targets and their locations is of high importance, but doing so is challenging because (a) the localization sensing infrastructure (e.g., surveillance cameras) may not be readily available or has been destroyed, and (b) visual inspection of human targets is restricted if not impossible. WIDESEE is designed to offer decision supports in such difficult settings.

In our application of human sensing, we aim to achieve the following two goals. The first is to detect the existence of human targets. The second is to identify the target's location if a presence is detected. We do not consider a multiple-device or multi-hop transmission scheme, because such a strategy requires a careful and complex setup process, which is often infeasible in emergency situations. As a proof-of-concept, WIDESEE is designed to be capable of detecting the presence of multiple human targets located in different rooms in the same building, but only localizing one target at a time. We leave the simultaneous localization of multiple targets as our future work.

2.3 Overview of WIDESEE

WIDESEE is a wide-range contactless human target sensing system built upon a single LoRa transceiver pair. The transceiver pair (both the transmitter and receiver) is carried by a drone so that WIDESEE can scan and sense a large area by flying the drone. Having a small, lightweight design for WIDESEE is essential to maintain a good endurance for the battery-powered drone.

WIDESEE operates by first transmitting the LoRa signal, and then capturing and analyzing the received resultant signal from the direct signal path and reflections off the target and surrounding objects. To detect the presence of a human target, WIDESEE models how a human activity like breathing, waving or ambulating affects the power spectral density (PSD) of the received signal. WIDESEE then tries to locate a detected human target by extracting and analyzing the target's direction-related information. As depicted in Figure 2, WIDESEE consists of three innovative components:

- A compact, *reconfigurable antenna system* to reduce the interference from uninterested areas. To prevent moving targets from being missed, the antenna should be able to adjust its direction and radiation pattern quickly. Our design is detailed at Section 3.1.
- A *data collection and antenna control system*, which includes a LoRa transceiver pair, a data collection subsystem, and a drone. The drone carries the LoRa transceiver pair and the data collection subsystems to fly around the target region. The collected LoRa signal data are sent back to a laptop (through a LTE network) to be processed on the ground. The antenna control system employs an Arduino board carried by the drone to configure the antenna radiation pattern accordingly. The details are described in Section 3.2.
- A *target detection and localization system*, which runs on a data processing platform, i.e., a laptop in our case. The system analyzes the collected data to detect and localize the human target. This is discussed in detail in Section 3.3.

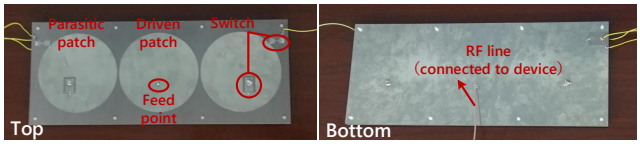

Figure 3: The fabricated antenna system on the receiver side.

3 SYSTEM DESIGN OF WIDESEE

WIDESEE leverages LoRa's long communication range and high penetration capability for sensing targets that are within a wide area or deep inside building structures. As discussed in Section 2.1, this advantage also brings in more interference from uninterested objects due to the larger sensing range. Overcoming this limitation requires novel design methodologies, analysis and processing algorithms.

3.1 Reconfigurable Antenna System

To reduce the interference, we look for innovations at the antenna side. Our first intuition is to employ a directional antenna at the receiver to narrow down the sensing region. However, commonly used horn directional antennas such as RFMAX [5] have a fixed radiation pattern and mechanically rotating the antenna orientation to focus on a region is too slow. Furthermore, the beamwidth offered by a horn antenna is usually not narrow enough [5]. An alternative is to use a phased-array antenna that can change the radiation pattern by adjusting the amplitude and phase of each antenna element, to achieve fast scanning with narrower beams [19, 25]. However, there is a problem for using a phased-array antenna with LoRa. The LoRa signal has a wavelength of 33 *cm* and to achieve a 25° beamwidth, the linear array will have a size of approximately 2 *m*. The resulted antenna design is not only expensive, but also too bulky to be fitted on a domestic drone.

We wonder if we could bring together the advantages of horn antenna (small size and low cost) and phased array (high resolution and scanning speed). In answer, we adopt a reconfigurable antenna approach [12], which is capable of switching the radiation pattern and frequency properties through adjusting its internal current flow distribution to offer a narrow beamwidth.

Specifically, we choose to use a parasitic-planar-patch antenna [29] for our reconfigurable antenna design. Figure 3 shows our reconfigurable antenna implementation that is used at the receiver side,

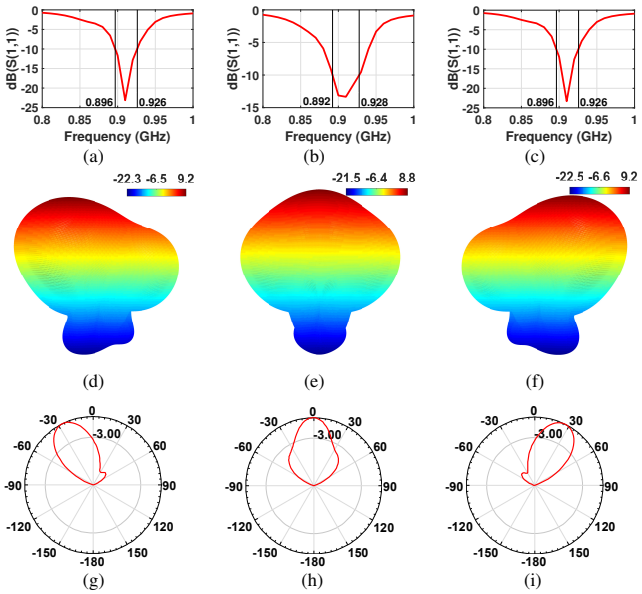

Figure 4: Frequency and radiation properties of our reconfigurable antenna system. Here (a-c), (d-f) and (g-i) respectively represent the frequency property, radiation pattern and normalized radiation pattern of mode1-3.

Table 1: Properties of our antenna system and a similar-sized RFMAX [5] – a popular horn directional antenna.

	Frequency range (MHz)	Gain (dBic)	Beamwidth (at 3 dB)	Size (cm^3)
WIDESEE (mode 1)	896-926	9.2	48°	
WIDESEE (mode 2)	892-928	8.8	45°	$20 \times 50 \times 1$
WIDESEE (mode 3)	896-926	9.2	48°	
RFMAX	902-928	9	70°	$26 \times 26 \times 5$

which consists of a driven patch in the center and two parasitic patches on both sides. Beam steering is achieved by manipulating the status of the parasitic patches to act either as reflectors (when shorted to ground) or directors (when not shorted to ground). The radius of each patch is 78 mm. Two shorting pins are shorted to ground from each parasitic patch, to ensure that the currents can flow from the parasitic patches to the ground according to the RF switching configuration. Two SMP1345 PIN diode switches are soldered on the parasitic patch layer close to each of the shorting pins and the RF/direct-current (DC) input. Each diode occupies a small space of around 2×2 mm. The PIN diode is achieved by using a resistance (1.5 Ω) and a capacitor (1.5 pF) for ON and OFF states, respectively. The resulting antenna system is small (20×50 cm) and has a comparable weight to a similar-sized horn directional antenna (< 1 kg), but has the advantage of quickly switching the radiation patterns. It costs us less than 300 USD to build the antenna and its control system, and we expect the price to be significantly reduced during massive production.

Figure 4 shows the frequency and radiation properties of our antenna system. Our current implementation supports three different radiation modes. We use an Arduino board to switch between the three modes in a round-robin fashion, where switching occurs every

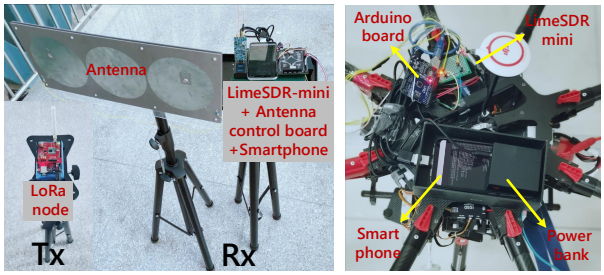

(a) The transceiver pair (b) Data collection and control

Figure 5: We use a DJI S1000 to carry the LoRa transceiver pair (a) and the data collection/control subsystem (b).

10 ms. We empirically determined this switching frequency which is sufficient for sensing human targets. This is based on the observation that the human body movements often have a frequency less than 10 Hz [17].

Table 1 compares our antenna system (in three different modes) against a similar-sized RFMAX [5] – a widely used horn directional antenna. From the table, we see that the frequency range and gain of our antenna system for the three modes are comparable to those of RFMAX, but our design has the advantages of offering quick radiation pattern switching and a narrower beamwidth. These advantages make our antenna system more suitable for target sensing with LoRa. Note that, the total radiation angle range of our system is twice RFMAX's, and the radiation pattern switching is much quicker (i.e., 10 ms) than horn antenna which requires mechanical rotation for direction change.

3.2 Data Collection and Antenna Control System

As depicted in Figure 2, we use a consumer drone to carry the transceiver pair and its control and data collection modules.

3.2.1 Transceiver pair. Our LoRa transceiver pair is shown in Figure 5 (a). We use an off-the-shelf device, Semtech SX1276 [6], with an omnidirectional antenna as the LoRa signal transmitter. The transmitter sends signals in a continuous mode at 890 MHz frequency – the best working frequency of our reconfigurable antenna system. At the receiver end, we use LimeSDR-mini (a software defined radio board [4]) as the LoRa gateway to collect signal at a sampling rate of 250 KHz through running the GNU radio software development toolkit [2]. We connect the board to our reconfigurable antenna (see Section 3.1) through one of its RF connectors, and to an Android smartphone (with 8G of RAM and 128G of storage) via a USB 3.0 port.

The receiver end works as follows. After initializing the LimeSDR-mini board, the antenna control software running on the Arduino board continuously switches among the three radiation modes of the antenna, at a frequency of 10 ms. The LimiSDR-mini board collects the signal samples at each radiation mode, which are read by the smartphone to be transferred (labeled with the radiation modes) to a laptop via LTE connection for data processing. In this way, WIDESEE can detect and localize targets within an interested area covered by each radiation mode. Note that it is possible for our target detection and localization algorithms to run on the smartphone or an

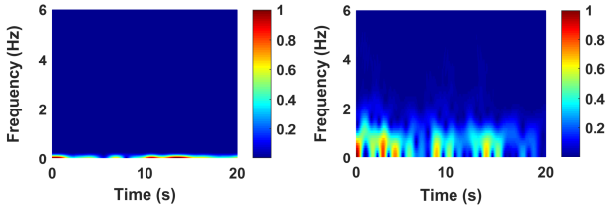

(a) Without human target. (b) With a moving human target.

Figure 6: Comparison of the PSD of the received signal when there exists no human target (a) and a moving target (b). The PSD patterns in two scenarios differ significantly. WIDESEE exploits this observation to detect the presence of human targets.

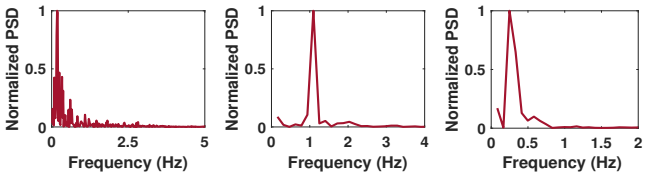

(a) Ambulating. (b) Waving. (c) Stationary.

Figure 7: Frequency distribution of signal changes caused by three states of a human target. Different states lead to different signal frequency distributions.

embedded device to remove the need of data transfer, and we leave this as our future work.

3.2.2 Drone System. We use a DJI S1000 drone [7] to increase the area a single transceiver pair can effectively cover. As illustrated in Figure 5 (b), the LimeSDR-mini, smartphone, Arduino board are put on top of the drone and are powered by a 5200 mAh portable power bank with a 2.4 A output. We employ the collision avoidance system provided by DIJ to avoid drone collision with obstacles. The drone is controlled by software running on a laptop, programmed through the DJI software development kits. One limitation of the drone system is that it can not operate for a long time when loaded with the devices and one battery charge can support around 15 minutes of flight. Our future implementation will look into reducing the drone's load by running the data collection and antenna control software on a single computing device (e.g., the Arduino board), which can be powered directly by the drone's battery. Multiple drones can be utilized to alleviate this power-hungry issue.

3.3 Target Detection and Localization System

We develop a set of algorithms to process the collected LoRa signal data to detect and localize human targets. The process of detection and localization works as follows. We first pre-process the received signal to remove the noises caused by the drone's vibration artifacts. We then exploit the power spectrum density (PSD) of the processed signal to detect the presence of human targets. The PSD is calculated as the Fast Fourier transform of signal amplitudes' self-correlation. Note that our detection mechanism can detect the presence of target no matter one or multiple targets are present in the sensing area. After detecting the presence of a moving target, we apply the localization algorithm to estimate the location of the target whose reflection is strongest at that time (note that during localization stage, we let the device hover in place). With the device mobility, we can detect and locate multiple targets successively. As we have previously discussed, WIDESEE needs to effectively handle the multipath effects and location ambiguities brought in by using only one LoRa transceiver pair.

3.3.1 Vibration noise elimination. Vibrations of a flying drone inevitably introduce noise to the received LoRa signals. To remove the introduced noise, we exploit the observation that the motion artifacts brought by a drone are within a frequency range between 60 Hz and 150 Hz, which is different from the lower frequency range of a human body movement ($< 10\ Hz$). Therefore, we first use a low-pass filter (i.e., second-order Butterworth low pass filter with a cutoff frequency of 10 Hz) to remove the high-frequency motion artifacts in the frequency domain and then convert the filtered signal back to the time domain to be processed in the next stage. Our evaluation in Section 4 shows that this is a simple yet effective strategy.

3.3.2 Human target detection. Human activities like hand waving and walking will alter the wireless propagation paths and lead to the change of signal amplitude at the receiver [10]. Prior work shows that when no human target is present, the received signal can be approximated as the superposition of constant signals and the white Gaussian noise, yielding an invariant PSD with time [41]. By contrast, the PSD of the received signal resulted from a moving human target, will lead to fluctuations on the measured signal. As an example, consider Figure 6 drawn from our own experiments. It illustrates the difference in the PSD with and without a moving human target. When no human target is present (Figure 6 (a)), the PSD of the received signal remains stable with time and close to 0 Hz, while when a moving target presents (Figure 6 (b)), the PSD fluctuates at low frequencies ($0 - 10\ Hz$). Our work exploits this signal characteristic to detect the presence of a human target – if the measured PSD frequency and its variance are both below a threshold (empirically set to 0.1 Hz in our case), we consider there is no human target; otherwise, we conclude that someone (with movements) is in the sensing area.

In this work, we focus on detecting human targets with large movements: ambulating or waving in-place. We are also able to detect a stationary breathing target when there is no obstacle between the transceiver pair and the target, or the obstacle is thin (see Section 4.2.3). Figure 7 illustrates the normalized PSD of the reflected signals of these three states (ambulating, waving and stationary) from a human target in a controlled environment. The diagram shows that different states exhibit different characteristics in the frequency domain, which can be used to identify and differentiate these states. In particular, human breath and waving present strong, dense PSD with a frequency range of 0.1-0.6 Hz and 1-4 Hz, respectively. By contrast, the PSD distribution of an ambulating human target is more spread apart, mainly due to the human target's randomized ambulatory trajectory pattern and uncorrelated movements of multiple body parts.

3.3.3 Ambulating Target Localization. Once an ambulating human target is detected, we focus on identifying the location of the

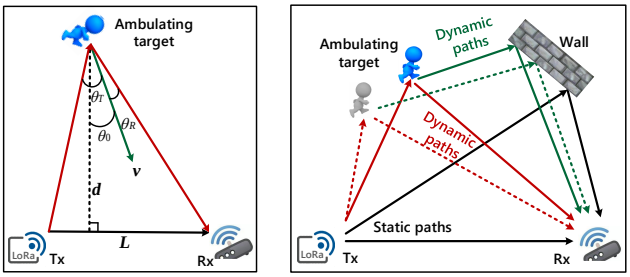

Figure 8: (a) shows the setup of moving target localization. Similar to the linear virtual array constructed by moving receiver. The moving target also can emulate a linear array. (b) presents the superposition signal of multiple paths.

target. One of the technical challenges in LoRa-based target localization is that the multipath in LoRa is more severe than that in other signals (e.g., WiFi). Even though we utilize the narrower beam antenna at the receiver, the multipath within the sensing area can be still substantially strong, which negatively impacts target localization. To address the multipath issue for localization, previous work has investigated various techniques, such as analyzing the AoA information [52], frequency hopping based on accurate channel phase measurement [35, 40], and comparing ToF that requires large bandwidth and tight transceiver synchronization [33]. Unfortunately, these techniques are not applicable to our system because the maximum bandwidth of LoRa is only 500 KHz, and the asynchronism between LoRa node (Tx) and gateway (Rx) makes it difficult to extract stable phase readings from the received signal. Also, it is particularly difficult to achieve synchronization between LoRa node and gateway due to the cheap oscillator adopted. Because of the chirp modulation, LoRa can tolerate high frequency offset for commutation so high-accuracy oscillator is not needed.

In this work, we propose an amplitude-based anti-multipath method to localize a moving target. The foundation of our method is to extract direction-related information from signal amplitudes, inspired by a recent work by Karanam *et al.* [31]. By using the direction-related information for localization, we have the opportunity to remove the multipath effect that however is not addressed in [31]. In the following subsections, we first describe the basic concepts behind extracting the direction-related information when a target is moving. Then, we answer how to obtain target location information from the extracted direction-related information. Finally, we propose the solution to handle multipath.

Direction-related parameter estimation. Here we first describe the framework for estimating direction-related parameter in device moving scenario (target does not move), which can be used to deduce the direction-related parameter in target moving case (device does not move).

Considering a scenario in which we have one receiver that receives signals from K different sources. When the receiver moves along a straight line at a speed v, it can emulate a linear array. We can define the incoming angle of each signal source in far-field as θ_k, $k = 1, 2, ..., K$. Then, the signal received from the k^{th} source at time t can be expressed as $x_{t,k} = a_{t,k}e^{j(\mu_k + \frac{2\pi v t}{\lambda} cos\theta_k)}$ [21], where $a_{t,k}$ is the amplitude of the signal and μ_k is the signal phase at the initial time point (i.e., $t = 0$). Then, the signal received at the receiver at time t is a superposition of K signals, which can be written as:

$$y(t) = \sum_{k=1}^{K} a_{t,k}e^{j(\mu_k + \frac{2\pi v t}{\lambda} cos\theta_k)}. \quad (1)$$

Let us denote $R(\tau)$ as the self-correlation of the received signal amplitudes at delay τ. Then, $R(\tau)$ can be expressed as [21, 31]:

$$R(\tau) = C_A + \sum_{k=1}^{K-1}\sum_{j=k+1}^{K} C_{k,j} \cdot cos\left(2\pi\frac{v\tau}{\lambda}(cos\theta_k - cos\theta_j)\right), \quad (2)$$

where C_A is a constant term depending on the total signal power and $C_{k,j} = \frac{\pi a_{t,k}^2 a_{t,j}^2}{16\sum_{k=1}^{K} a_{t,k}^2}$, where $a_{t,k}^2$ is the signal power of k^{th} signal. It is noteworthy that $R(\tau)$ is consisted of a total of $\frac{K(K-1)}{2}$ harmonics. Each harmonic's frequency is related to the cosine of two sources' AoA (i.e., θ_k, θ_j, and $k = 1, 2, ..., K$, $j = 1, 2, ..., K$), which is given by:

$$\widetilde{f_{k,j}} = \frac{v}{\lambda}|cos\theta_k - cos\theta_j|. \quad (3)$$

Note that $cos\theta_k$ and $cos\theta_j$ are unknowns we are trying to obtain the values. These frequencies $\widetilde{f_{k,j}}$ can be obtained by the frequency estimation technique, such as the fast Fourier transformation of amplitudes' self-correlation followed by a peak magnitude detection.

For the target moving and transceiver fixed scenario shown in Figure 8 (a), the resultant signal is composed of reflection (Tx → target → Rx) from an ambulating human target and direct path (Tx → Rx). The resultant signal at time t can thus be written as:

$$y(t) = a_s e^{j\mu_s} + a_d e^{j(\mu_d + \frac{2\pi v t}{\lambda}(cos\theta_T + cos\theta_R))}, \quad (4)$$

where a_s and μ_s are the amplitude and phase of the direct path signal, a_d is the amplitude of the signal reflected from the moving target, μ_d is the initial phase ($t = 0$) of the reflected signal, v is the moving speed of the target, θ_T and θ_R are two angles marked in Figure 8 (a).

Equation (4) is a special case of Equation (1) with 2 sources ($K = 2$), $cos\theta_1 = 0$ and $cos\theta_2 = cos\theta_T + cos\theta_R$. The moving target can synthesize a transmitter array. We put $cos\theta_1$ and $cos\theta_2$ into Equation (3) to obtain the following:

$$\widetilde{f_{1,2}} = \frac{v}{\lambda}|0 - (cos\theta_T + cos\theta_R)|, \quad (5)$$

since v, θ_T and θ_R are unknowns in practice, we jointly estimate the direction-related parameter $|v(cos\theta_T + cos\theta_R)|$ as $\widetilde{f_{1,2}}\lambda$ according to Equation (5).

Localization ambiguity avoidance. By utilizing the $|v(cos\theta_T + cos\theta_R)|$ estimate from only one transceiver pair to localize the target, there exist severe localization ambiguities that stem from three aspects: (1) the absolute value symbol $|\ |$ applied to $v(cos\theta_T + cos\theta_R)$; (2) unknown distance d between the target and the Tx-Rx LoS link as shown in Figure 8 (a); and (3) unknown speed v and direction θ_0 of target movement. We show the localization result of a special case ($\theta_0 = 0$) in Figure 11 (a). We can see that even with $\theta_0 = 0$ to simplify the problem, there still exist ambiguities (the areas with red color). So it is difficult to obtain the target's true initial location.

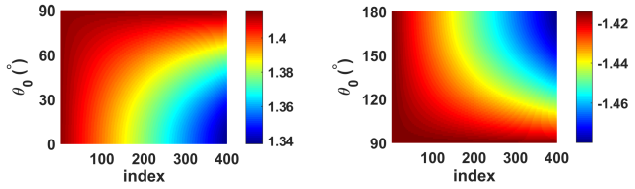

(a) Target moves towards LoS. (b) Target moves away from LoS.

Figure 9: The changing trend of $v(cos\theta_T + cos\theta_R)$ estimates at various target moving directions θ_0. It can be seen that the changing trend of $v(cos\theta_T + cos\theta_R)$ estimates from the 1st to m^{th} is always *decreasing* no matter the target moves towards LoS ($0° < \theta_0 < 90°$) or moves away from LoS ($90° < \theta_0 < 180°$).

In this paper, we solve this problem based on the facts that the target's moving trajectory is smooth and the velocity is a constant during a short period of time (e.g., $< 1\ s$). Specifically, we utilize multiple consecutive estimates of $v(cos\theta_T + cos\theta_R)$ with a sliding window of size w, and each estimation process requires samples collected in a time window of size τ. w and τ are empirically set as $0.25\ s$ and $1\ s$ in our system. To reduce the computational time, we reduce the sample rate from 250 KHz to 1 KHz for PSD calculation. We aim to solve five unknown parameters: $[\theta_{T1}, \theta_{R1}, \theta_0, d_1, v]$, where θ_{T1} , θ_{R1} and d_1 are the initial values of θ_T, θ_R and d respectively. Note that within a short period of time, v and θ_0 can both be considered as constants while θ_T, θ_R and d are changing. During the process of target movement within a short period of time, we keep estimating the 3 changing variables. For the m^{th} estimates, we can have the following two equations bellow:

$$\begin{cases} v(cos\theta_{Tm} + cos\theta_{Rm}) = \pm(\widetilde{f_{1,2}\lambda})_m \\ d_m(tan(\theta_0 + \theta_{Rm}) + tan(\theta_{Tm} - \theta_0)) = L \end{cases} . \quad (6)$$

Note that ± can be removed due to our observation as shown in Figure 9. We find that the changing trend of $v(cos\theta_T + cos\theta_R)$ estimates from the 1st to m^{th} are always *decreasing*. When the target moves towards transceiver pair, the values of $\cos\theta_T$ and $\cos\theta_R$ ($0° < \theta_T < 90°$, $0° < \theta_R < 90°$) are positive and the values decrease with angles θ_T and θ_R increasing. When the target moves away from the transceiver pair, the values of $\cos\theta_T$ and $\cos\theta_R$ ($90° < \theta_T < 180°$, $90° < \theta_R < 180°$) are negative and the values again decrease with angles increasing. So we delete another set of estimates that do not satisfy the condition of *decreasing* from the 1st to m^{th} estimates.

Consider the fact of trajectory smoothness and speed constancy over a short period of time, we can add the following constraints:

$$\begin{cases} \theta_{Tm} \approx \theta_{T1} + (m-1)\alpha \\ \theta_{Rm} \approx \theta_{R1} + (m-1)\beta \\ d_m \approx d_1 - v\tau(m-1)cos\theta_0 \end{cases} , \quad (7)$$

where α and β are constant but unknown. By incorporating Formula 7 into Formula 6, we find that when m reaches to 4, the number of equations ($2m = 8$) is larger than the number of unknowns (a total of 7 with 5 original unknowns and 2 newly introduced unknowns). Thus we are able to solve the unknowns with only 4 estimates of $|v(cos\theta_T + cos\theta_R)|$ as shown in Figure 10.

Since the equations are non-linear that can not be solved directly, an intuitive choice is to use Approximate Search algorithm. To avoid the local optimum issue and reduce time overhead, we adopt

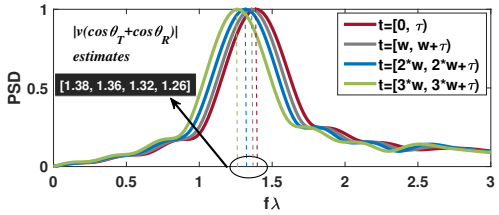

Figure 10: Four adjacent estimates of direction-related parameter $|v(cos\theta_T + cos\theta_R)|$. The estimates are the normalized frequencies corresponding to the peaks of PSD plots.

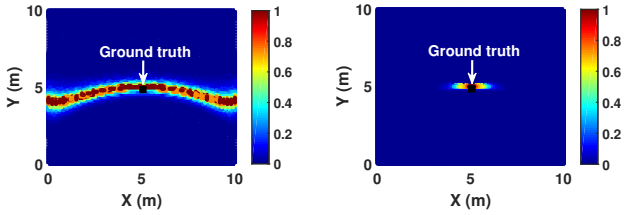

(a) Before ambiguity avoidance. (b) After ambiguity avoidance.

Figure 11: Localization ambiguity avoidance. The heatmap exhibiting the likelihood that how a partitioned grid is likely to be the initial location of the target. The coordinates of Tx and Rx are $(0, 0)$ and $(10, 0)$, the ground truth is highlighted with black square. From (a), we can see all grids of the reddest color result in the same value of $|v(cos\theta_T + cos\theta_R)|$, resulting severe localization ambiguities.

Particle Swarm and Global Search from Matlab Global Optimization Toolbox to achieve global optimum search for the set of non-linear equations. The principle is to obtain an initial search value close to the solution using particle swarm, then limit the objective function with fmincon's non-linear constraints, and finally use Global Search to obtain the solution. The computational complexity of the search algorithm is $O(N \times M)$, where N is the dimension of the particle swarm and M is the number of iterations. Figure 11 (b) shows that the initial localization result with our ambiguity avoidance scheme is close to the ground-truth.

Multipath interference elimination. Consider a typical multipath scenario shown in Figure 8 (b), we can see that the received signal at the receiver is a superposition of multiple signals, which can be written as:

$$\begin{aligned} y(t) = a_s e^{j\mu_s} + a_d e^{j(\mu_d + \frac{2\pi vt}{\lambda}(cos\theta_T + cos\theta_R)} \\ + a'_d e^{j(\mu'_d + \frac{2\pi vt}{\lambda}(cos\theta'_T + cos\theta'_R)}, \end{aligned} \quad (8)$$

where a_d, μ_d, θ_T and θ_R are the amplitude, initial phase ($t = 0$), angle parameters of the direct target reflection (Tx→target→Rx), respectively. To simplify representation, here we approximate the indirect target reflection (Tx→target→wall→Rx) as a new direct reflection from a virtual target (Tx→virtual target→Rx), with amplitude a'_d, initial phase ($t = 0$) μ'_d, direction parameters θ'_T and θ'_R. In such scenario, the $\widetilde{f\lambda}$ value set has $|v(cos\theta_T + cos\theta_R)|$ as well as $|v(cos\theta'_T + cos\theta'_R)|$ and $|v(cos\theta_T + cos\theta_R) - v(cos\theta'_T + cos\theta'_R)|$ components. Since the resultant static component (contains direct path)

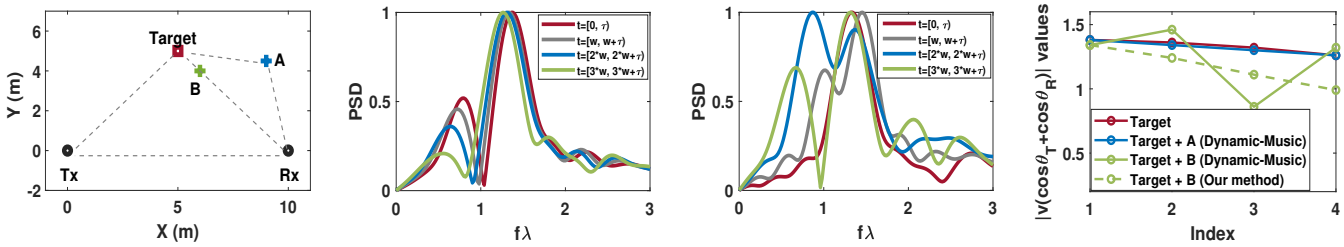

(a) Setup.

(b) PSD plots with interfering object at location A.

(c) PSD plots with interfering object at location B.

(d) $|(v(cos\theta_T + cos\theta_R))|$ estimates.

Figure 12: Multipath interference presentation. The figure shows that past AoA based multipath removal solution fails when the interfering object is close to the connecting line between target and receiver/transmitter (like at location B). Our approach has the ability to mitigate the problem.

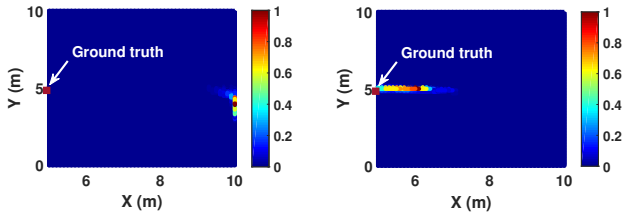

(a) Using Dynamic-Music.

(b) Using our approach.

Figure 13: Localization errors of using past (5.1 m) and our (1 m) multipath elimination approaches, when an interfering object locates at point B as shown in Figure 12 (a).

Figure 14: Evaluation scenarios. We evaluate WIDESEE in an open square (a), an underground parking garage (b), and a middle floor of a 17-floor building (c). The testing area is on one side of the transmitter-receiver line in all of the experiments.

is much stronger than the reflections, we can lock the two dominant $\widetilde{f}\lambda$ estimates as $|v(cos\theta_T + cos\theta_R)|$ and $|v(cos\theta'_T + cos\theta'_R)|$.

To distinguish the target corresponding $|v(cos\theta_T + cos\theta_R)|$ value from the $|v(cos\theta'_T + cos\theta'_R)|$ estimate shown in Figure 12 (b-c), existing solutions (e.g., Dynamic-Music) exploit the fact that the direct target reflected path is stronger than the indirect target reflected path [34, 46, 52] due to the shorter path of former, so they consider the $\widetilde{f}\lambda$ value of larger magnitude as the direct target reflection resulted $|v(cos\theta_T + cos\theta_R)|$.

This approach can be effective when the interfering object (at location A in Figure 12 (a)) is far away from the connecting line between target and receiver/transmitter. We can see that the four estimates of $|v(cos\theta_T + cos\theta_R)|$ decrease monotonically as shown in Figure 12 (d) when there is one interfering object at location A. Figure 12 (b) shows the PSD plots and the position ($\widetilde{f}\lambda$) of the peak is the estimate. We can see that for 4 consecutive time window, the ($\widetilde{f}\lambda$) is decreasing. These results are similar to the case when there is no interfering object. However, when the interfering object (at location B in Figure 12 (a)) is close to the connecting line between target and receiver/transmitter, the $|v(cos\theta_T + cos\theta_R)|$ estimates show remarkable shifts as shown in Figure 12 (c) and (d) and thus fail to localize the target. To mitigate this problem, instead of taking the peak value position $\widetilde{f}\lambda$ shown in Figure 12 (c) as $|v(cos\theta_T + cos\theta_R)|$, we take the average of two positions corresponding to largest and second largest peak values as $|v(cos\theta_T + cos\theta_R)|$ if we find the four estimates are not decreasing monotonously and the second largest peak value is larger than 50% of the largest peak value. Figure 12 (d) shows that by using our methods to obtain the new $|v(cos\theta_T + cos\theta_R)|$, the 4 estimates now decrease monotonously and match the no-interfere estimates much better than those obtained with the Dynamic-Music method. The localization error of our method (1 m) is much lower than that of Dynamic-Music method (5.1 m).

4 EVALUATION

4.1 Experimental Setup and Roadmap

We performed two sets of field experiments to evaluate WIDESEE in detecting and localizing human targets: field experiments without a drone and field experiments with a drone.

4.1.1 Field experiments without a drone. We would like to provide a quantitative evaluation first to justify our design choices, and to identify the research opportunities and limitations of LoRa sensing. To this end, we evaluate how the distance between transmitter and receiver affects the sensing range of LoRa in Section 4.2.1. In Section 4.2.2, we report the performance of our antenna design for detecting moving human targets and compare it with two alternative designs using omni- and horn-directional antennas. We then evaluate LoRa's penetration capability in detecting three different human activities in Section 4.2.3, before reporting the localization accuracy of our system in Section 4.2.4. Finally, in Section 4.2.5, we evaluate the impact of the human target's walking speed on detection and localization accuracy. Controlled experiments were performed on the ground for detecting a single moving human target with the LoRa transceiver pair placed 1 m above the ground. Later in the field study, we use the drone to carry the transceiver pair.

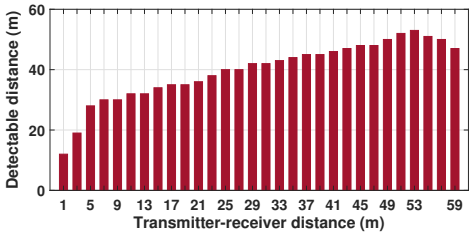

Figure 15: Impact of the transmitter-receiver distance on the detectable distance (sensing range). WIDESEE can detect a moving object with a distance to the transceiver pair of up to 53 m in an open square.

4.1.2 File study with a drone. In the field study, we use a drone to carry the LoRa transceiver pair to detect and locate a human target in the building shown in Figure 14 (c). We report the performance for detecting the presence of human targets and the accuracy for localizing a human target with different drone speeds. The results are given in Section 4.3.

4.1.3 Evaluation metric. We calculate the accuracy for detecting the presence of a human target as:

$$Accuracy = \frac{1}{C}\sum_{c=1}^{C}(1 - |\frac{H_{m,c} - H_{t,c}}{H_{t,c}}|), H_{m,c}, H_{t,c} = \{0, 1\}$$

where C is the number of tests, $H_{m,c}$ and $H_{t,c}$ are the outputs of WIDESEE and the ground-truth in the cth test respectively.

4.2 Field experiments without a drone

4.2.1 Sensing range under different transmitter-receiver distances. In this experiment, we varied the transmitter-receiver distance, i.e., the distance between the transmitter and the receiver, from 1 m to 59 m at a step size of 2 m. The tests were conducted in the open square shown in Figure 14 (a). In each transceiver pair setting, we asked a target to walk along the vertical bisector of the transceiver pair 100 times with a walking distance of 3 m each time, starting from a randomly chosen position. Note that we moved the starting point further from the transceiver pair each time, until we fail to detect the user at that point. We consider a position to be detectable if we can correctly detect the user at that position for over 90% of the time. We calculated the distance between each detectable position and the middle point of the transceiver pair link to find the largest-possible sensing distance (i.e., sensing range) for a given setting.

Figure 15 shows how the transmitter-receiver distance affects the sensing range of WIDESEE. We see that the sensing range in general grows as the transmitter-receiver distance increases. However, it reaches a plateau with a detectable distance of 53 m. This suggests that WIDESEE can achieve a sensing range of 53 m for a moving target in a relatively ideal environment (an open square). Such a sensing range is a significant improvement over WiFi, RFID and mmWave-based systems, which have a sensing range below 6 m [47, 51, 55]. However, we believe there is a potential to further increase this sensing range with careful signal processing considering the kilometer-level communication range and we leave it as important future work.

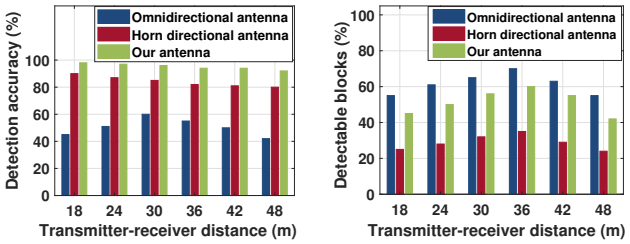

(a) Detection accuracy. (b) Detectable area.

Figure 16: Comparing the detection accuracy (a) and region (b) between our approach and alternative directional antennas with a similar size. Our antenna design gives the best trade-off between the detection accuracy and range.

4.2.2 Evaluation of our antenna system. This experiment is designed to evaluate the performance of our antenna system in human target detection. We compare our design against two alternative designs which use an omnidirectional [1] and a horn directional (RFMAX [5]) antenna with a similar size. Our testing area is an open square with a size of 42×48 m^2 depicted in Figure 14 (a). We divided the testing area into a grid of 224 blocks, 3×3 m^2 for each block. Like the previous experiment, we asked a human target to choose any block and then move within the block naturally. We ensure that each block was tested at least once.

Figure 16 shows that our design presents the best trade-off between the detection accuracy and area coverage. In this experiment, we report the number of detectable blocks. Note that this is different from the evaluation in Section 4.2.1, where we are interested in the longest-possible distance for detecting a target that is always on the perpendicular bisector of the transceiver pair. In this experiment, most of the blocks are not on the perpendicular bisector of the transceiver pair. As we increase the transmitter-receiver distance beyond 36 m, we see a decrease in the number of detectable blocks. This is mainly due to the directionality of the receiver antenna.

While RFMAX, the horn directional antenna achieves the second-best detection accuracy, it can detect the least number of blocks. The omnidirectional antenna, on the other hand, can cover more blocks, but it achieves the poorest detection accuracy due to its high sensitivity to the surrounding interference. The sensing range achieved by our antenna is relatively large due to the signal focusing and radiation direction switching, and it delivers a much higher detection accuracy for all settings. The better detection accuracy of our approach is largely attributed to its narrower beam, which in turn leads to a stronger signal and at the same time less interference from non-target objects.

4.2.3 Penetration test. We also evaluate WIDESEE's ability to penetrate the walls. Experiments were conducted in the underground garage as shown in Figure 14 (b) and the second floor of our test building shown in Figure 14 (c). Our evaluation includes four settings – no wall and wall made of reinforced concrete with three different thicknesses (26 cm, 52 cm and 94 cm) between the target and the transceiver pair. In the through-wall experiment, we placed the transceiver pair 1.5 m away from the wall.

Figure 17 shows the results. As expected, the thinner the obstacle between the target and the transceiver pair, the deeper WIDESEE

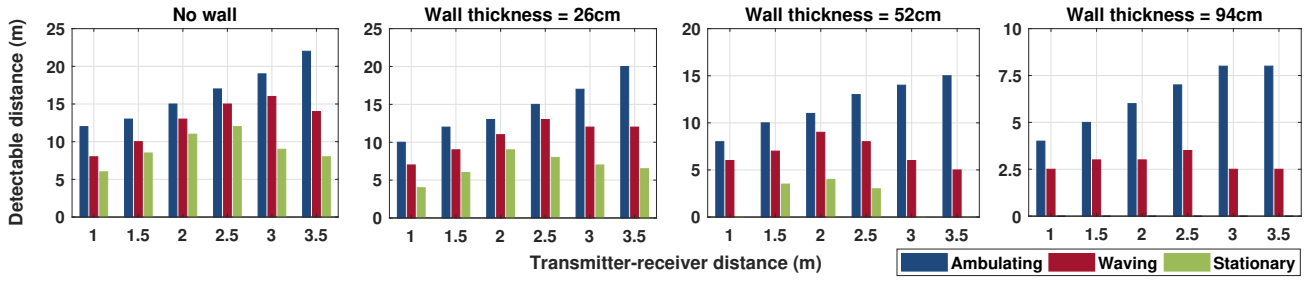

Figure 17: Penetration test. WIDESEE can detect a stationary human target who is behind a wall with a thickness of 52cm, and WIDESEE can detect a moving/walking target deeper inside a wall.

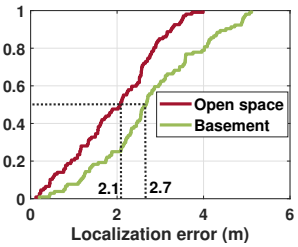

Figure 18: CDF plots of the localization error in two large scenarios ($10 \times 25\ m^2$) with different densities of multipath.

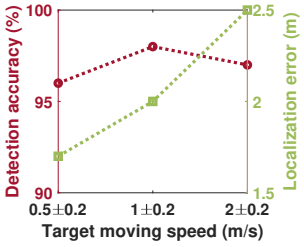

Figure 19: Impact of target moving speed. The target's moving speed has little impact on detection, but it affects localization.

can successfully detect the target. We observe the target's activity also has a significant impact on the detectable distance. If the target is ambulating or waving, WIDESEE can successfully detect the target up to 15 m and 13 m, respectively. WIDESEE can also detect a stationary target with just respiration. However, the detection distance is limited and depends on the thickness of the wall. This is not surprising, as the smaller the activity and the thicker the wall is, the weaker the received signal strength will be. For our experiments, a 20 cm increase in the wall's thickness would reduce the received signal strength by around 29 dB. Nonetheless, the results show that WIDESEE can accurately detect a human target moving or waving deep inside the building.

4.2.4 Localization accuracy in different multipath environments. We report how multipath impacts localization accuracy in this section. Our evaluation environments are the open square (Figure 14 (a)) and basement parking garage (Figure 14 (b)). As can be seen from Figure 14 (b), the basement is supported by many pillars and hence has rich multipath. The test areas in both environments are of the same size ($10 \times 25\ m^2$), and we set the transmitter-receiver distance as 10 m. We divided the testing area into 125 blocks, where each block has a size of $2 \times 1\ m^2$. For each block, a target was asked to walk following predefined straight lines that have 0°, 30°, 45°, 60° or 90° degrees with respect to the transmitter-receive line. For each line, the user walked for around 2 s, starting from the center of a block. Figure 18 plots the cumulative distribution function (CDF) of the localization error across our 125 experimental trials. This diagram shows that for over 50% of our test cases, the localization error is within 2.1 m and 2.7 m in the open square and the basement, respectively. Such accuracy would be good enough for locating a human target in many application scenarios, demonstrating the great potential of sensing using a single LoRa transceiver pair.

We conduct another experiment to show the tracking accuracy of our system in a smaller area. This experiment was performed in a smaller room located in the building shown in Figure 14. The room has a size of $8 \times 10\ m^2$. In this experiment, the transmitter-receiver distance is set as 6 m. The target was asked to walk along the trajectory of five letters "BCIMO". The recovered trajectories (dots) and the ground-truth trajectories (solid lines) are shown together in Figure 20. WIDESEE achieves a median localization error of 52 cm, which is comparable to the 32 cm error achieved in IndoTrack - a state-of-art WiFi tracking system with dense deployment [51]. This experiment shows that WIDESEE is able to track the target at higher accuracy in a smaller-size area.

4.2.5 Impact of the target's moving speed. This experiment studies the effect of the target's walking speed on detection and localization. We consider three walking speeds: slow ($0.5 \pm 0.2\ m/s$), average ($1 \pm 0.2\ m/s$) and fast ($2 \pm 0.2\ m/s$). We conducted the experiments in the open square shown in Figure 14 (a).

Figure 19 shows that the target's moving speed has little impact on target detection, but it does affect the localization accuracy. We observe a localization error of 1.7 m, 2 m, and 2.5 m when the target was moving at slow, average, and fast speeds respectively. This is largely attributed to the body motions (e.g., arm swing) – the faster the walking speed is, the more drastic the body movement will be – a more drastic body movement makes it harder to satisfy the conditions that we use for localization (see Equation 7).

4.3 Building-scale Field Study

In this field study, we employ WIDESEE with a drone (see also Figure 2) to perform building-scale sensing. The task is to detect and track a human target located on the 9th floor of a 17-floor building structure with a size of $20 \times 42 \times 85\ m^3$ (Figure 14 (c)). Note that this new building had no occupant at the time of our experiment. The thicknesses of the concrete walls and glass windows are 40 cm and 5 cm, respectively. The transceiver pair was carried by a drone in this experiment. The distance between the transmitter and the receiver is 2 m. Ten student volunteers participated in this study, serving as the target. Figure 21 shows the experimental setup. The students were arranged into three groups to perform stationary (breathing) (2

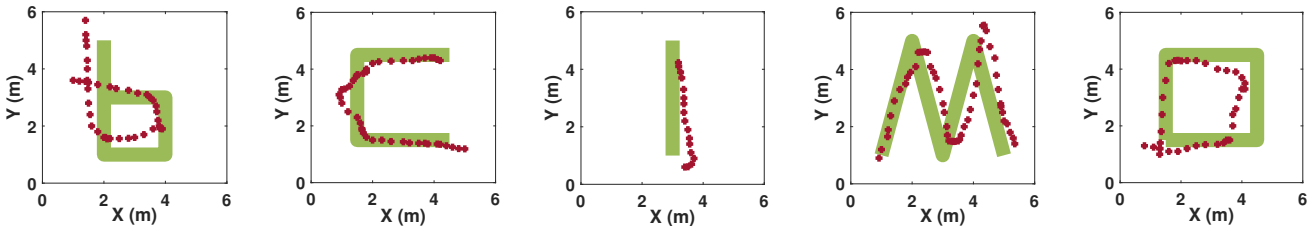

Figure 20: Tracking results in a smaller room with size of $6 \times 8\ m^2$. The median tracking error of WIDESEE is $52\ cm$, which is comparable with a state-of-the-art that utilizes two WiFi transceiver pair[51].

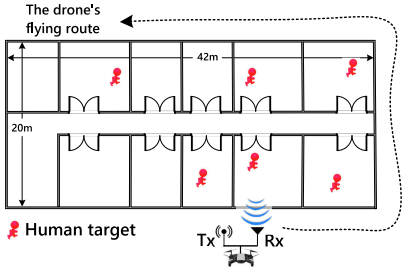

Figure 21: Building-scale experimental setup.

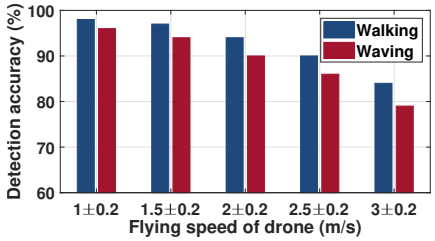

Figure 22: Target detection accuracy in building-scale field study, with various drone's flying speeds.

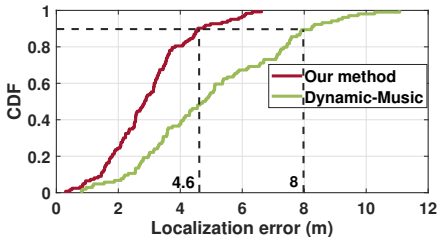

Figure 23: CDF plot of the localization error given by our and Dynamic-Music's multipath elimination schemes.

students), waving (4 students) and walking (4 students) activities, and are located in rooms on the same floor. We manually controlled the drone to fly to an initial position of the 9^{th} floor, and used the software-based control module (Section 3.2.2) to control the drone's fly. We varied the flying speed of the drone in the experiments.

4.3.1 Detecting human presences. Figure 22 shows the detection accuracy for each human target who was walking and waving. When the drone was flying at a low speed of $1 \pm 0.2\ m/s$, WIDESEE can successfully detect 98% and 96% of the human targets who were walking and waving respectively. As expected, the detection accuracy decreases as the drone's speed increases, but WIDESEE is still able to detect the target most of the time when the target was walking or waving. WIDESEE is unable to detect the stationary (breathing) target in this study when the device is on a drone and the target is pretty far away ($> 5\ m$) from the device with a $40\ cm$ wall made of reinforced concrete in between. How to improve the detection accuracy for stationary human targets with respiration sensing is one important direction of our future work. However, our current implementation would already be useful for disaster rescue to detect conscious survivors, many of whom tend to wave to attract the attention of rescuers.

4.3.2 Localization accuracy. Once we have detected a moving target, we hover the drone for 2 seconds to collect the target movement information, and apply the localization algorithms described in Section 3.3.3 to estimate the target position. Figure 23 compares the localization error of our approach with Dynamic-Music [52]. As we can see, our approach delivers a better localization accuracy over Dynamic-Music. It reduces the localization error from $8\ m$ to $4.6\ m$ for over 90% of the test cases. Although the $4.6\ m$ localization error is intuitively large, it allows us to identify which room or roughly which area of a building a human target is located. This is particularly useful in disaster rescue where we critically need to narrow down the search area for survivors.

5 DISCUSSIONS

As the first attempt in applying LoRa signals for sensing, there is room for improvement and further work. We discuss a few issues here.

Non-moving target localization. We are able to detect non-moving human target through sensing his/her respiration or in-place activities such as waving. Note that the sensing range of through-wall respiration sensing is still limited, since the signal attenuation caused by walls is significant and the signal variation induced by respiration movement (around $5\ mm$ chest displacement) is small and can easily be buried in noise. We plan to explore the feasibility of utilizing beamforming technology [24, 53, 59] to amplify the weak reflected signal to increase the respiration sensing range in the future. Careful signal processing with an antenna array is another promising direction to increase the sensing range as demonstrated in Farsense [56].

Target localization with device movements. In this paper, we can localize the target with a single pair of transceiver when the target is moving. Note that our system can not localize the target when the sensing device is also moving. This is because we remove the dynamic multipath interference based on the fact that dynamic multipath reflected twice is much weaker than direct target-reflected signal. However, if the transmitter/receiver is also moving, the original static path will also become dynamic path, which may be stronger than the direct target-reflected signal and then we can not get rid of the effect of dynamic multipath in this case, resulting in large localization errors.

Multiple-target sensing. We are not able to detect and localize multiple targets simultaneously since the target-reflected signals get mixed together and it is extremely challenging to separate the mixed signals with a limited channel bandwidth. In our future work, we plan to employ antenna array to focus the transmission power at one direction and also exploit the blind signal separation algorithm [16, 54] to separate mixed signals for multi-target sensing.

Despite these limitations, WIDESEE moves an important step toward enabling wide-area contactless sensing. We believe WIDESEE provides valuable reference for future research in this field.

6 RELATED WORK

Our work is broadly related to the literature in two areas.

6.1 Human Activity Recognition

Computer-vision-based human activity sensing techniques have enabled mature applications. For instance, Kinect [8] and Leap Motion [3] can achieve fine-grained human gesture tracking. However, these systems are sensitive to lighting condition and the monitoring angle and cannot work when the target is blocked or behind a wall. Wearable sensor-based solutions overcome the above limitations [13, 20, 32] but still bring in inconvenience to users as they require instrumenting the users. However, it would be unrealistic to assume every target has a working wearable in emergencies.

Compared to vision or wearable-based solutions, wireless-signal-based human activity recognition systems can penetrate walls and do not require the user to carry or wear a device. Early work in this area use multiple transceiver pairs to construct a 3D lattice of wireless links to identify the presence of human movements [44]. Later work try to use a single device equipped with multiple antennas to realize activity recognition. For example, WiSee can differentiate nine commonly seen body gestures with the help of machine learning techniques [42]. The effectiveness of the learning based methods depends on the quality of the training data, but obtaining high quality training data remains costly and non-trivial. For example, CrossSense [23] requires collecting thousands of samples to learn a single activity recognition model at one given environment. WIDESEE avoids the pitfalls of a learning-based approach by developing analytical models for activity recognition. It requires significantly less effort for collecting data samples and can be portable to different environments.

Recent studies also show it is possible to sense the respiration [9, 15, 18], heart rate [9], or even emotion [38] using wireless signals. However, prior approaches only work at a small scale (e.g., the room-level) and would require dense deployment to work on a large area. WIDESEE builds upon these past foundations of human activity modeling, to extend the scope of contactless human sensing for wide areas with a LoRa transceiver pair. Our work aims to close the gap of wireless sensing for disaster rescue in the urban areas, as well as terrorist search and security surveillance.

6.2 Indoor Localization and Tracking

There is an intensive body of work in localizing and tracking objects [10, 11, 22, 28, 51, 59]. Prior work can be broadly grouped into two categories: device-based and device-free approaches.

A device-free approach has the advantage of not requiring the end-user to carry a device. By lifting the limitation of carrying a device, device-free methods can target a wider range of applications when compared to the device-based counterparts. WIDESEE thus follows a device-free (contactless) approach.

Target location and tracking can be realized through a range of wireless signal characteristics, including AoA [22, 33], ToF [32, 36], and the signal amplitude [30]. An amplitude-based approach is simple and cost-efficient, but it suffers from poor localization accuracy (especially in non-line-of-sight conditions) – due to additional signal attenuation resulted from obstacles and severe amplitude fluctuation due to rich multipath indoors. Methods using phase information such as AoA can effectively separate multipaths, and a good resolution and accuracy would require a large antenna array at the receiver. ToF-based methods are not ideal either, because they are limited by the frequency bandwidth.

WIDESEE is the first attempt to realize contactless wide-area sensing with a single LoRa transceiver pair. It does so by combing the long-communication LoRa signal and the mobility of the drone. However, achieving the goal requires overcoming two challenges: (1) the serve multipath effects when using single LoRa transceiver pair, and (2) the hurdle for not having available phase or ToF information on LoRa. Inspired by [31], WIDESEE extracts direction-related information from amplitude measurements for localization, but it advances prior work by relying on a single instead of multiple transceiver pairs. WIDESEE employs a set of new algorithms to remove the localization ambiguity caused by one transceiver pair. WIDESEE also leverages and refines existing multipath removal methods [52]. The result is a promising solution using a single transceiver pair for wide-area contactless sensing, which could potentially open up many new research opportunities.

7 CONCLUSIONS

This paper has presented WIDESEE, a hardware-software system that can perform wide-area wireless sensing using just one transceiver pair. WIDESEE utilizes LoRa signals to achieve better through-wall penetration and larger sensing range. To further widen the sensing area, WIDESEE employs drones to carry the transceiver to improve the sensing coverage. The combination of single LoRa transceiver pair and device mobility, however, brings new challenges of severe interference and sensing ambiguities (e.g., localization). To address these challenges, we design a set of techniques at the hardware and software layers, which can be applied to many wireless sensing applications. We believe WIDESEE moves an important step towards wide-area wireless sensing, and is highly attractive in real-world emergency scenarios like disaster rescue and terrorist search.

ACKNOWLEDGMENTS

This work was supported in part by the National Natural Science Foundation of China (NSFC) under Grant Numbers 61572402, 61602382 and 61872294, the Key Project of Research Plan of Shaanxi under Grant 2018SF-369, the Science and Technology Innovation Team Support Project of Shaanxi under Grant 2018TD-026, and the International Science and Technology Cooperation Project under Grant 2019KWZ-05.

REFERENCES

[1] https://m.tb.cn/h.3CfHtz1?sm=3a9293/. 2017.
[2] Gnuradio. https://www.gnuradio.org/. 2018.
[3] Leap motion. https://www.leapmotion.com/. 2015.
[4] Limesdr mini. https://limemicro.com/products/boards/limesdr-mini/. 2018.
[5] Rfmax s9028pcr antenna. https://www.atlasrfidstore.com/rfmax-s9028pcrj-s8658prj-rhcp-indoor-rfid-antenna-fcc-etsi/. 2015.
[6] Semtech sx1276 transceiver. http://www.semtech.com/wireless-rf/rf-transceivers/sx1276/. 2016.
[7] Spreading wings s1000. https://www.dji.com/cn/spreading-wings-s1000/. 2015.
[8] X-box kinect. http://www.xbox.com/. 2015.
[9] Fadel Adib, Mao Hongzi, Zachary E. Kabelac, Dina Katabi, and Robert C Miller. Smart homes that monitor breathing and heart rate. In *ACM CHI*, 2015.
[10] Fadel Adib, Zach Kabelac, and Dina Katabi. Multi-person localization via rf body reflections. In *USENIX NSDI*, 2015.
[11] Dhekne Ashutosh, Chakraborty Ayon, Sundaresan Karthikeyan, and Rangarajan Sampath. Strackio: Tracking first responders inside-out. In *USENIX NSDI*, 2019.
[12] Jennifer T. Bernhard. Reconfigurable antennas. *Synthesis Lectures on Antennas*, 2(1):1–66, 2007.
[13] Chen Bo, Vivek Yenamandra, and Kannan Srinivasan. Tracking keystrokes using wireless signals. In *ACM MobiSys*, 2015.
[14] Gao Chuhan, Li Yilong, and Zhang Xinyu. Livetag: Sensing human-object interaction through passive chipless wifi tags. In *USENIX NSDI*, 2018.
[15] Zhang Fusang, Zhang Daqing, Xiong Jie, Wang Hao, Niu Kai, Jin Beihong, and Wang Yuxiang. From fresnel diffraction model to fine-grained human respiration sensing with commodity wi-fi devices. In *ACM UbiComp*, 2018.
[16] Hassanieh Haitham, Abari Omid, Rodriguez Michael, Abdelghany Mohammed, Katabi Dina, and Indyk Piotr. Fast millimeter wave beam alignment. In *ACM SIGCOMM*, 2018.
[17] Zeng Hansong and Zhao Yi. Sensing movement: Microsensors for body motion measurement. In *Sensors*, 2011.
[18] Wang Hao, Zhang Daqing, Ma Junyi, Wang Yasha, Wang Yuxiang, Wu Dan, Gu Tao, and Xie Bing. Human respiration detection with commodity wifi devices: do user location and body orientation matter? In *ACM UbiComp*, 2016.
[19] Aboulnasr Hassanien and Sergiy A. Vorobyov. Phased-mimo radar: A tradeoff between phased-array and mimo radars. *IEEE Transactions on Signal Processing*, 58(6):3137–3151, 2010.
[20] Wang He, Tsung Te Lai, and Romit Roy Choudhury. Mole: Motion leaks through smartwatch sensors. In *ACM MobiCom*, 2015.
[21] William C. Jakes. *Microwave mobile communications*. Wilery-IEEE Press, 1994.
[22] Xiong Jie and Kyle Jamieson. Arraytrack: a fine-grained indoor location system. In *USENIX NSDI*, 2013.
[23] Zhang Jie, Tang Zhanyong, Li Meng, Fang Dingyi, Nurmi Petteri, and Wang Zheng. Crosssense:towards cross-site and large-scale wifi sensing. In *ACM MobiCom*, 2018.
[24] Wang Jingxian, Zhang Junbo, Saha Rajarshi, Jin Haojian, and Kumar Swarun. Pushing the range limits of commercial passive rfids. In *USENIX NSDI*, 2019.
[25] Gjengset Jon, Xiong Jie, McPhillips Graeme, and Jamieson Kyle. Phaser: Enabling phased array signal processing on commodity wifi access points. In *ACM MobiCom*, 2014.
[26] Wang Ju, Jiang Hongbo, Xiong Jie, Kyle Jamieson, and Xie Binbin. Lifs: Low human-effort, device-free localization with fine-grained subcarrier information. In *ACM MobiCom*, 2016.
[27] Wang Ju, Xiong Jie, Chen Xiaojiang, Jiang Hongbo, Rajesh Krishna Balan, and Fang Dingyi. Tagscan: Simultaneous target imaging and material identification with commodity rfid devices. In *ACM MobiCom*, 2017.
[28] Wang Jue and Dina Katabi. Dude, where's my card? rfid positioning that works with multipath and non-line of sight. 2013.
[29] Muzammil Jusoh, Tamer Aboufoul, Thennarasan Sabapathy, Akram Alomainy, and Muhammad Ramlee Kamarudin. Pattern-reconfigurable microstrip patch antenna with multidirectional beam for wimax application. *IEEE Antennas and Wireless Propagation Letters*, 13(1933):860–863, 2014.
[30] Wu Kaishun, Jiang Xiao, Yi Youwen, Min Gao, and Lionel M. Ni. Fila: Fine-grained indoor localization. In *IEEE INFOCOM*, 2012.
[31] Chitra R. Karanam, Belal Korany, and Yasamin Mostofi. Magnitude-based angle-of-arrival estimation, localization, and target tracking. In *IEEE IPSN*, 2018.
[32] Palanivel Kodeswaran, Ravindranath Kokku, Madhumita Mallick, and Sayandeep Sen. Demultiplexing activities of daily living in iot enabled smarthomes. In *IEEE INFOCOM*, 2016.
[33] Manikanta Kotaru, Kiran Joshi, Dinesh Bharadia, and Sachin Katti. Spotfi:decimeter level localization using wifi. In *ACM SIGCOMM*, 2015.
[34] Zhang Lingyan, Gao Qinghua, Ma Xiaorui, Wang Jie, Yang Tingting, and Wang Hongyu. Defi: Robust training-free device-free wireless localization with wifi. *IEEE Transactions on Vehicular Technology*, 67(9):8822–8831, 2018.
[35] Shangguan Longfei and Kyle Jamieson. The design and implementation of a mobile rfid tag sorting robot. In *ACM MobiSys*, 2016.
[36] Alexander Mariakakis, Souvik Sen, Jeongkeun Lee, and Kyu Han Kim. Sail: single access point-based indoor localization. In *ACM MobiSys*, 2014.
[37] Sara Minaeian, Jian Liu, and Young-Jun Son. Vision-based target detection and localization via a team of cooperative uav and ugvs. *IEEE Transactions on systems, man, and cybernetics: systems*, 46(7):1005–1016, 2016.
[38] Zhao Mingmin, Fadel Adib, and Dina Katabi. Emotion recognition using wireless signals. In *ACM MobiCom*, 2017.
[39] Rajalakshmi Nandakumar, Shyamnath Gollakota, and Nathaniel Watson. Contactless sleep apnea detection on smartphones. In *ACM MobiSys*, 2015.
[40] Rajalakshmi Nandakumar, Vikram Iyer, and Shyamnath Gollakota. 3d localization for sub-centimeter sized devices. In *ACM SenSys*, 2018.
[41] A. Michael Noll. *Principles of Modern Communications Technology*. Artech House, 2001.
[42] Pu Qifan, Jiang Siyu, and Shyamnath Gollakota. Whole-home gesture recognition using wireless signals. In *ACM SIGCOMM*, 2013.
[43] Yun Sangki, Chen YiChao, Zheng Huihuang, Qiu Lili, and Mao Wenguang. Strata: Fine-grained acoustic-based device-free tracking. In *ACM MobiSys*, 2017.
[44] Li Sun, Souvik Sen, Dimitrios Koutsonikolas, and Kyu-Han Kim. Widraw: Enabling hands-free drawing in the air on commodity wifi devices. In *ACM MobiCom*, 2015.
[45] Vamsi Talla, Mehrdad Hessar, Bryce Kellogg, Ali Najafi, Joshua R. Smith, and Shyamnath Gollakota. Lora backscatter: Enabling the vision of ubiquitous connectivity. 2017.
[46] Liu Tao, Wan Lei, Qin Zhenquan, Qian Chen, and Zhou Xin. Passive acoustic localization based on cots mobile devices. In *IEEE ICPADS*, 2018.
[47] Wei Teng and Zhang Xinyu. mtrack: High-precision passive tracking using millimeter wave radios. In *ACM MobiCom*, 2015.
[48] Teodor Tomic, Korbinian Schmid, Philipp Lutz, Andreas Domel, Michael Kassecker, Elmar Mair, Iris Lynne Grixa, Felix Ruess, Michael Suppa, and Darius Burschka. Toward a fully autonomous uav: Research platform for indoor and outdoor urban search and rescue. *IEEE robotics & automation magazine*, 19(3):46–56, 2012.
[49] Deepak Vasisht, Swarun Kumar, and Dina Katabi. Decimeter-level localization with a single wifi access point. In *USENIX NSDI*, 2016.
[50] Wang Wei, Alex X. Liu, and Sun Ke. Device-free gesture tracking using acoustic signals. In *ACM MobiCom*, 2016.
[51] Li Xiang, Zhang Daqing, Qin Lv, Xiong Jie, Li Shengjie, Zhang Yue, Mei Hong, Li Xiang, Daqing Zhang, and Lv Qin. Indotrack: Device-free indoor human tracking with commodity wi-fi. *Proceedings of the Acm on Interactive Mobile Wearable and Ubiquitous Technologies*, 1(3):72, 2017.
[52] Li Xiang, Li Shengjie, Zhang Daqing, Xiong Jie, and Mei Hong. Dynamic-music: accurate device-free indoor localization. In *ACM UbiComp*, 2016.
[53] Fan Xiaoran, Ding Han, Li Sugang, Sanzari Michael, Zhang Yanyong, Trappe Wade, Han Zhu, and Howard Richard E. Energy-ball: Wireless power transfer for batteryless internet of things through distributed beamforming. *ACM UbiComp*, 2018.
[54] Xie Yaxiong, Xiong Jie, Li Mo, and Kyle Jamieson. md-track: Leveraging multi-dimensionality inpassive indoor wi-fi tracking. 2018.
[55] Zou Yongpan, Xiao Jiang, Han Jinsong, Wu Kaishun, Li Yun, and Ni Lionel M. Grfid: A device-free rfid-based gesture recognition system. *IEEE Transactions on Mobile Computing*, 16(2):381–393, 2017.
[56] Zeng Youwe, Wu Dan, Xiong Jie, Yi Enze, Gao Ruiyang, and Zhang Daqing. Farsense: Pushing the range limit of wifi-based respiration sensing with csi ratio of two antennas. In *ACM UbiComp*, 2019.
[57] Ma Yunfei, Nicholas Selby, and Fadel Adib. Drone relays for battery-free networks. In *Proceedings of the Conference of the ACM Special Interest Group on Data Communication*, pages 335–347. ACM, 2017.
[58] Ma Yunfei, Nicholas Selby, Manish Singh, and Fadel Adib. Fine-grained rfid localization via ultra-wideband emulation. In *ACM SIGCOMM Posters and Demos*, 2017.
[59] Ma Yunfei, Luo Zhihong, Steiger Christoph, Traverso Giovanni, and Adib Fadel. Enabling deep-tissue networking for miniature medical devices. In *ACM SIGCOMM*, 2018.